Cellulose
https://doi.org/10.1007/s10570-025-06716-3

ORIGINAL RESEARCH

Characterization of adhesive bonded nonwovens made from blends of agro-waste, cotton, and viscose fibers

Ramya Kanagaraj · Amutha Karuppuchamy · Sukanya Devi Ramachandran

Received: 3 April 2025 / Accepted: 31 July 2025

Abstract Nonwoven fabrics find wide array of applications in technical textile sector. Most of these nonwovens are made with synthetic fibers that do not biodegrade thereby leading to environmental pollution. On the other side some agricultural waste contains potential ligno-cellulosic fibers that could be effectively used in making nonwovens. This study aims at developing nonwovens by utilizing agro-waste fibers such as wild turmeric (*Curcuma aromatica*) petiole fiber (WTPF) and banana (*Musa paradisiaca*) core stem fiber (BCSF) blended with natural cellulosic fiber (cotton) and regenerated cellulosic fiber (viscose). Natural fiber nonwovens are heavy and bulky compared to the synthetic counterparts. Hence the selected fibers are blended in seven different ratios and converted into a web by carding followed by needle punching. It is then adhesive bonded by coating with sericin gel, a bio-polymer known for its antibacterial properties, followed by hot calendaring. The developed nonwoven fabrics were analysed for their physical, mechanical, structural, and morphological properties. The areal density (GSM) of the lightest among the developed nonwovens is 95 while the heaviest one is 160. The samples highly varied in thickness ranging from 0.71 to 0.83 mm and fiber packing density from 8.42 to 15.92%. The tear strength along machine and cross directions varied from 864 to 112 and 736 to 80 gf respectively. The porosity and air permeability ranged from 84.08 to 91.58% and 23.12 to 95.62 $cm^3/cm^2/s$. Based on the properties, the developed nonwoven fabrics could be utilized in various technical textile applications, including hygiene textiles, agro-textiles, geotextiles, and so on.

R. Kanagaraj (✉) · A. Karuppuchamy
Department of Textiles and Apparel Design, Bharathiar University, Coimbatore, India
e-mail: ramya.dtad@buc.edu.in

A. Karuppuchamy
e-mail: amuthatad@buc.edu.in

S. D. Ramachandran
Department of Textile Technology, Kumaraguru College of Technology, Coimbatore, India
e-mail: sukanyadevi.r.txt@kct.ac.in

Published online: 03 September 2025

Graphical Abstract

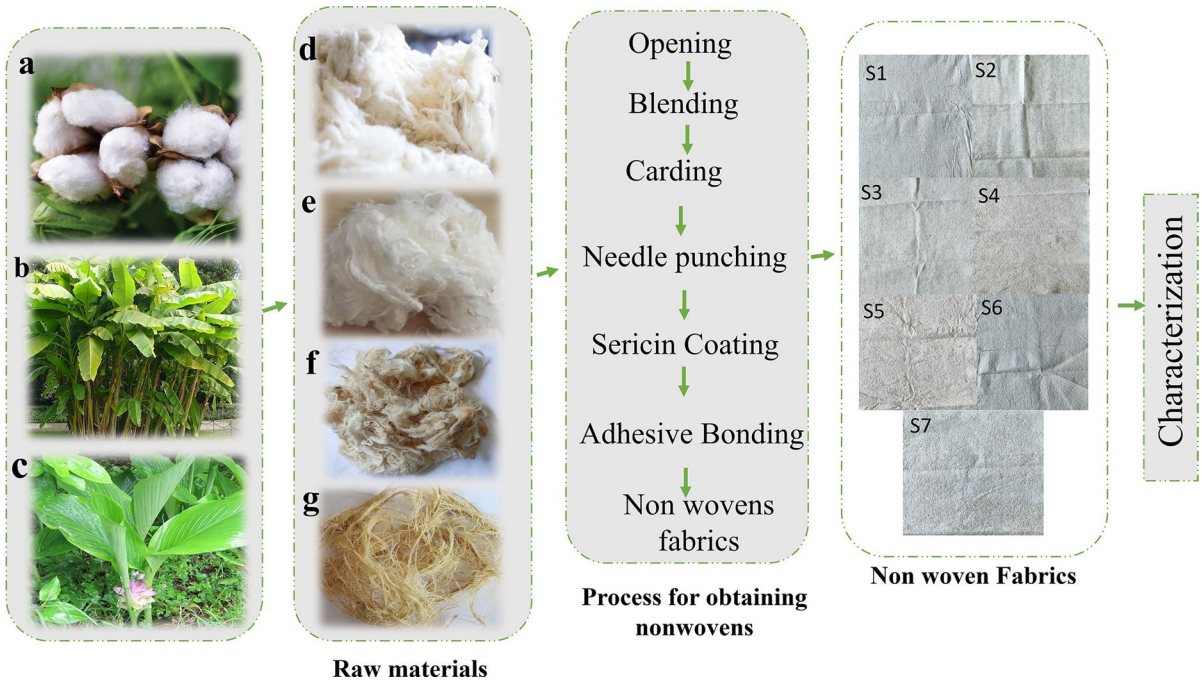

Keywords Agro-waste fibers · Biodegradable · Needle-punching · Hygiene textiles · Ligno-cellulosic fibers · Sustainable textiles

Introduction

Hygiene products are often manufactured using nonwoven fabrics-textile materials formed by bonding fibers together through mechanical, thermal, or chemical processes. Unlike traditional fabrics, these porous structures are created directly from fibers or molten polymers, eliminating the need to spin fibers into yarn before forming the fabric (Mitchell 2019).

The nonwoven manufacturing process originated in 1936, pioneered by Dr. Carl Nottebohm. Initially, it utilized natural fibers such as wool, cotton, and jute, along with natural binders like starch and rubber. Over time, however, the industry shifted toward synthetic fibers and binders due to their enhanced performance properties (Santos et al. 2021). Despite their advantages, nonwoven products with high synthetic content present significant disposal challenges, contributing to global environmental concerns. Disposable nonwoven wipes are widely used across various industries. Industrial and professional applications often employ wet-laid pulp/polypropylene (PP) spun-laced fabrics, while household and hygiene wipes are typically made from spunbonded or dry-laid fabrics, bonded chemically or thermally (Bhat and Parikh 2010).

In response to global sustainability trends, the nonwoven sector increasingly incorporates natural ligno-cellulosic fibers. These fibers are valued for their biodegradability, renewability, low cost, and non-toxicity (Temesgen 2018). Natural fibers such as cotton, silk, flax, jute, and regenerated cellulose fibers like viscose are commonly used in hygiene, medical, and disposable nonwoven products due to their softness, absorbency, and biodegradability. Additionally, agricultural residues and agro-waste fibers-such as banana stem, wild turmeric petiole, and maize tassel-are gaining attention as sustainable raw materials that convert crop waste into valuable textile fibers (Amutha et al. 2020).

Silk is a natural biomaterial composed primarily of two proteins: fibroin (inner layer) and sericin (outer layer). It is known for its excellent biodegradability, biocompatibility, cell adhesion, and

water retention properties, making it highly suitable for biomedical and cosmetic applications. Furthermore, silk exhibits antioxidant, antimicrobial, UV-protective, and moisture-absorbing properties, and can accelerate wound healing (Fatahian et al. 2018). Silk consists of approximately 97% protein, with the remaining 3% comprising waxes, carbohydrates, pigments, and minerals. It can be processed into various forms-such as sponges, films, gels, fibers, webs, nonwoven fabrics, and beads-to serve a wide range of applications (Kim et al. 2023). Silk nonwoven fabrics are typically produced by binding silk webs-made from degummed waste silk-with reclaimed sericin. This eco-friendly and cost-effective method requires minimal investment and promotes sustainable production (Nivedita and Mishra 2016).

The growing awareness of hygiene practices, especially during global health crises such as the COVID-19 pandemic, has accelerated the adoption of medical wet wipes for various applications, from wound care to personal hygiene (Gaminian et al. 2024). These wipes, typically made from nonwoven fabrics composed of natural or synthetic fibers, offer convenient and effective solutions for skin and surface cleaning. The medical wet wipes market is also benefiting from innovations in fiber technology (Shaikh et al. 2023).

The present study investigates the suitability of blending agro-waste, ligno-cellulosic fibers such as banana core stem fiber, and wild turmeric petiole fiber with cotton – a superior and comfort fiber for many applications, and viscose – a regenerated cellulosic fiber widely used in biodegradable textile applications for developing sericin-coated nonwoven fabrics intended for technical textile applications. The banana core stem fiber and wild turmeric petiole fiber are characterized by higher cellulosic content and crystallinity, porous and multi-fibrillar structure, relatively low denier and roughness compared to other ligno-cellulosic fibers, and good tensile strength making them suitable for nonwoven fabrication. The research involves fiber extraction, blending, and the formation of nonwoven fabrics through adhesive bonding techniques. Sericin, a biopolymer derived from silk, is applied as a coating to enhance the structural integrity, functional properties, and biodegradability of the fabrics. The coated nonwovens are comprehensively characterized using various techniques, including morphological analysis via field emission scanning electron microscopy (FESEM), functional group identification through Fourier transform infrared (FTIR) spectroscopy, and evaluations of tensile strength, air permeability, moisture absorption, thermal conductivity, and biodegradability.

This study highlights the potential of these skin-friendly nonwovens to replace conventional synthetic materials in health care products, while also offering advantages in diverse technical applications-including hygiene textiles, filtration, geotextiles, and industrial absorbents-due to their superior sustainability and performance.

Materials and methods

Materials

Cotton and viscose fibers were procured from suppliers in Tirupur, India. Sericin powder was obtained from silk hank dyers in Sirumugai, India. Banana core stems (*Musa paradisiaca*) were collected from a farmland in Coimbatore, India. Wild turmeric biomass was sourced from organic farm in Sathyamangalam, India.

Extraction of selected fibers

The fiber extraction process for wild turmeric petioles (Ramya Kanagaraj 2024), and banana core stems (Karuppuchamy et al. 2024) were carried out following the methods detailed in the respective studies. The Fig. 1 shows extraction process of selected fibers.

Physical and mechanical properties of WTPF and BCSF

The fiber length of the WTPF samples ranged from 20–40 cm for long fibers and 1–5 cm for short fibers, with a diameter of approximately 20 µm as observed through FESEM analysis. The densities of WTPF-1 and WTPF-2 fibers were found to be 1.31 g/cm^3 and 1.45 g/cm^3, respectively. Their tenacity values were found to be 1.39 g/den and 1.56 g/den (Ramya Kanagaraj 2024). In comparison, the banana core stem fiber (BCSF) had a denier of 1.53, a tenacity of

Fig. 1 Extraction process of wild turmeric petiole and banana core stem fibers **a** wild turmeric plant **b** stem **c** fiber extraction **d** wild turmeric petiole fiber **e** banana plant **f** banana core stem **g** fiber extraction **h** banana core stem fiber

Table 1 Nomenclature and blend ratios of nonwoven fabrics

Nomenclature	Viscose (%)	Cotton (%)	BCSF (%)	WTPF (%)
S 1	-	50	25	25
S 2	25	50	-	25
S 3	-	25	50	25
S 4	25	25	50	-
S 5	25	25	25	25
S 6	-	25	25	50
S 7	25	-	25	50

35.21 g/tex, and a density of 0.984 g/cm^3. However, the length of BCSF was not measured manually due to its fragile nature and characteristics such as tenderness, short length, brittleness, and low strength (Karuppuchamy et al. 2024). The chemical composition and mechanical properties of both fibers could be understood from the findings reported in the cited literature.

Nonwoven fabrication

The properties of nonwoven fabrics largely depend on the characteristics of the fibers and the manufacturing process. Processing 100% banana core stem fiber (BCSF) and wild turmeric petiole fiber (WTPF) during web formation is challenging, as these fibers tend to break and cause the web to fall apart during carding. To overcome this, they are blended with fibers such as cotton and viscose. The nomenclature and blend ratios of the developed nonwoven fabrics are presented in Table 1.

Preparation of needle punched nonwoven fabrics

The WTPF fibers are pre-cut to a length of 1 to 2 cm to facilitate even blending with the other selected fibers. To prevent fiber damage the fibers are manually opened. Seven different fiber blends of BCSF, WTPF, cotton, and viscose are prepared in the required weight ratios, as shown in Table 1. The blended fibers are then processed in a nonwoven production unit equipped with a TRY TEX carding machine, round drums, and a needle punching machine. For each ratio, the fibers are blended and fed in to the carding

machine to form a web. The web is fed again in to the carding machine to obtain better blending and a more even web. The web is then needle punched. Needle punching was carried out using a Dilo (Germany) needle punching machine at a density of 300 punches/cm^2 and a speed of 257 cycles/min, as recommended by (Govindaraju and Jagannathan 2018). The process was performed on a 70 cm-wide needle loom equipped with regular barbed needles arranged in staggered rows. A needle penetration depth of 12 mm was applied on both sides to ensure deep fiber interlocking and effective entanglement. To further enhance the tensile strength and uniformity of the fabric, double-sided needle punching was employed for all nonwoven samples.

Sericin coating and bonding of nonwoven fabrics

Raw sericin powder (0.5 g) is dissolved in 100 mL of water using the autoclave method at 200 °C for 10 min, forming a gel-like sericin solution. The nonwoven samples are then immersed in this solution for 15 min to ensure uniform absorption. To enhance sericin uptake, the fabric is passed through a two-bowl padding mangle, which aids in uniform impregnation. Excess sericin is removed during padding, and the treated nonwoven fabric is dried at room temperature.

After drying, the fabric undergoes hot calendaring to improve fiber bonding and increase strength. During calendaring, the nonwoven fabric is passed between heated rollers set at 130 °C at a pressure of 1.5 MPa. The bonding rollers operate at a speed of 6 m per minute for 3 s. The application of heat and pressure enhances the adhesion of sericin to the fibers, resulting in a stable and durable nonwoven fabric. The Fig. 2 shows the nonwoven development process.

Characterization of nonwoven fabric samples

The nonwoven fabrics were conditioned for 24 h under controlled atmospheric conditions (20 ± 2 °C and 65 ± 2% relative humidity). After conditioning, the samples were subjected to various performance evaluations, all carried out under the same environmental parameters.

Sericin add-on (%)

The sericin add on percentage was evaluated to estimate the amount of sericin deposited on the fabric surface after treatment. The following formula is used.

$$\text{Sericin add on}\,(\%) = \left[W_1 - W_2/W_2\right] \times 100 \qquad (1)$$

where.

W_1 = Weight of sericin coated nonwoven.

W_2 = Weight of untreated (needle punched) nonwoven fabric.

FTIR analysis

Fourier transform infrared (FTIR) spectroscopy is a powerful analytical technique used to characterize the chemical composition of nonwoven fabrics. This method provides valuable insights into the molecular structure and functional groups present in the fabric,

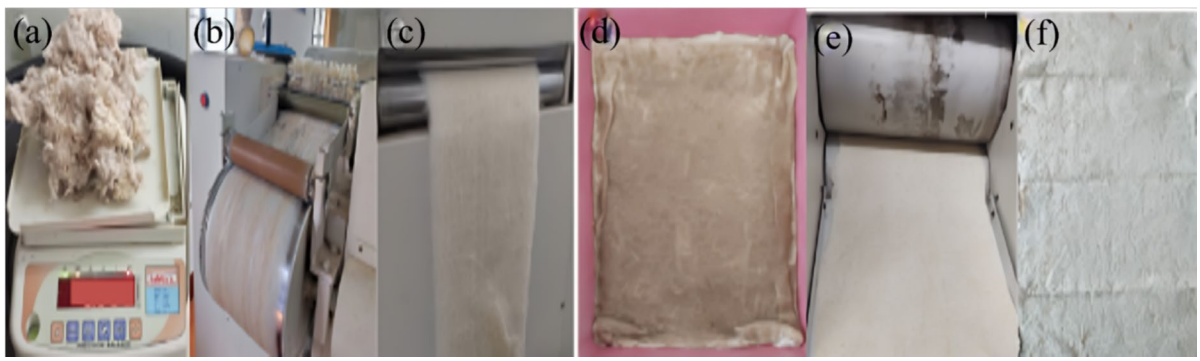

Fig. 2 Nonwoven development (a) weighing the fibers (b) carding process (c) needle punching (d) sericin coating (e) adhesive bonding (f) developed sample

which are crucial for understanding its performance and suitability for various applications.

In this analysis, nonwoven fabric samples are cut into small pieces and prepared using the KBr pellet method, where the fabric is finely ground and mixed with potassium bromide (KBr) to form a transparent pellet. The sample is then analyzed using a Shimadzu IR Prestige 21 FTIR spectrometer, with infrared radiation applied within a wavelength range of 500 cm^{-1} to 4000 cm^{-1}.

Areal density

The areal density (mass per unit area) was determined following the ASTM D3776/D3776M standard. Each nonwoven fabric sample was cut from five different locations using a round GSM cutter. The samples were then accurately weighed using an electronic balance, and the average value was calculated.

Thickness

The thickness of the nonwoven fabrics was measured according to the ASTM D1777-96 (2019) standard. An analog thickness gauge, known for its reliability and precision, was used to determine fabric thickness. This gauge can measure up to 10 mm with an accuracy of 0.01 mm, providing highly precise readings for various fabric types. The nonwoven fabric sample was securely placed on the device's anvil, while the pressure foot applied a controlled force when lowered onto the specimen. The thickness reading was recorded from the dial. Measurements were taken at multiple points across the fabric, and the average thickness was calculated.

Bulk density

Bulk density is the weight per unit volume of the nonwoven fabric expressed in kg/m^3. It is a crucial property for understanding the fabric's compactness and porosity. Bulk density is calculated using Eq. (2):

$$\text{Bulk Density}\left(kg/m^3\right) = \text{Mass per unit area}\left(g/m^2\right)/\text{Thickness(mm)} \quad (2)$$

where thickness is measured in millimetres and areal density in grams per square meter (Jhanji et al. 2015).

Fiber packing density

Fiber packing density is a key parameter in evaluating nonwoven fabrics, as it provides insights into how densely the fibers are packed within a given volume. It is calculated using Eq. (3) (Mao and Russell 2015):

$$\text{Fiber packing density}\ (\%) = \left[\text{Bulk Density}\left(kg/m^3\right)/\text{Density of the fiber}\left(kg/m^3\right)\right] \times 100 \quad (3)$$

Porosity

Porosity is defined as the ratio of the total void space in a material to its bulk volume. It is a critical parameter in assessing fabric comfort and the physical properties of technical textiles (Elnashar 2005). The volume per unit area represents the space occupied by the material per unit of surface area. It is a key factor in understanding how much material is distributed within a specific area (Mao and Russell 2015).

The porosity (P) of the nonwoven fabric is calculated using Eq. (4):

$$P\ (\%) = \left[1 - \text{Fiber packing density}\right] \times 100 \quad (4)$$

Liquid absorbency

The liquid absorbency of nonwoven fabrics was tested according to the ISO 9073–6:2000 standard. Test samples were cut from five different locations, and their initial weight (M_0) was measured using an electronic balance. Each sample was then placed in a petri dish filled with the liquid medium. The sample was immersed approximately 20 mm below the liquid surface and left for 60 ± 1 s. After immersion, the sample was removed, hung vertically, and allowed to drain for 120 ± 3 s.

Finally, the sample was weighed again to obtain the final mass (M_a). The liquid absorbency capacity was calculated using Eq. (5) (Thilagavathi et al. 2020).

$$\text{Liquid absorbency capacity} = \frac{M_c - M_0}{M_0} \times 100 \quad (5)$$

where:

M_0 = Initial mass of the sample (g).

M_c = Final mass of the sample after absorption (g).

Vertical wicking

The vertical wicking test was conducted following the AATCC TM 197–2011 standard method. Samples measuring 25 mm × 170 mm were cut from different areas of the nonwoven fabric. These samples were then suspended vertically and immersed in a solution containing red food colour to a depth of 10 mm. The wicking height was recorded at time intervals of 5, 10, 15, 20, 25, and 30 min. The rate of liquid movement along the fabric was visually assessed and documented.

Air permeability

The air permeability of the nonwoven fabric samples was measured according to the ASTM D737 standard. The test was conducted using a head area of $10cm^2$ and a pressure difference of 100 Pa. To ensure accuracy and consistency, three samples from each nonwoven fabric type were tested, and the average air permeability value was calculated.

Bursting strength

The bursting strength of the nonwoven fabric samples was measured in kg/cm^2 according to ASTM D3786 using a diaphragm bursting strength tester. For each sample type, five different test positions were selected, and the average bursting strength was calculated.

Tear strength

The tear strength of the nonwoven fabric samples was evaluated following the ASTM D1424 standard method. Two sets of samples were prepared: one in the machine direction and the other in the cross direction. The dimensions of the sample is 100 mm × 75 mm, with a 20 mm deep slit cut at the centre of one edge, perpendicular to the testing direction.

Tear strength measurements were taken in both directions, and the average tear strength values were calculated using Eq. (6):

$$\text{Mean tearing strength(gf)} = K \times \text{Mean value of scale reading} \quad (6)$$

where K is the weight constant, with values: A = 16, B = 32, C = 64, D = 128 and K = 16 is used for this study.

Surface morphology

The surface morphology of the nonwoven fabric samples was analyzed using a field emission scanning electron microscope (FESEM) from TESCAN, model MIRA3 XMU, equipped with an EDAX system by Gatan, model 3View 2XP. To enhance conductivity, the samples were coated with a thin layer of gold using a vacuum spray-coater. The analysis was performed at an acceleration voltage of 15 kV. This technique provides high-resolution imaging, enabling detailed examination of the fiber arrangement, bonding, porosity, and overall surface texture of the nonwoven fabric.

pH analysis of adhesive bonded nonwoven fabric

The pH analysis of the nonwoven samples was carried out following the guidelines outlined in ISO 3071:2020. The experiment was conducted under controlled laboratory conditions using a LabQuest orbital shaker for sample agitation at 150 rpm for 60 minutes. Each nonwoven sample was prepared by cutting the material into small pieces and accurately weighing approximately 2 grams. The samples were then subjected to aqueous extraction by mixing with distilled or deionized water at a material-to-liquor ratio of 1:50 (i.e. 2 grams of fabric in 100 mL of water). This mixture was stirred continuously using a mechanical shaker for 60 minutes at room temperature (25±2 °C) to ensure thorough extraction of any water-soluble components. After extraction, the solution was filtered to remove any suspended fibers or particles. The pH of the resulting filtrates was then measured using a calibrated digital pH meter

at 25 °C. This method ensures reliable and consistent evaluation of the surface pH, which is particularly important for materials intended for skin-contact applications.

Soil burial analysis

To assess the biodegradability of the nonwoven fabric samples, a soil burial test was conducted using normal garden soil. As per ISO 11721 standards, the pH of the soil was maintained within the range of 5.0 to 7.0 to simulate natural environmental conditions. Three different burial durations were selected to represent both short and longer degradation intervals (30, 90, and 120 days). The 120 days was considered a long-term exposure duration based on prior literature.

For each test condition, three replicates were prepared per fabric type to ensure data reliability. The fabric samples were cut into square dimensions (5 cm × 5 cm) and accurately weighed using a precision balance before burial. These were referred to as initial weights. The fabric samples were then buried in soil pits at a depth of approximately 10 cm and the soil was compactly closed to natural decomposition conditions. After completion of each burial interval (30, 90, and 120 days), the samples were carefully excavated.

Post-removal, the samples were gently rinsed twice with a 30:70% v/v ethanol/water solution to remove soil particles and prevent microbial contamination. The rinsed samples were thoroughly air-dried at room temperature and reweighed to determine the weight loss percentage. The unburied fabric samples were used as control samples for comparison to assess the extent of biodegradation (Sülar and Devrim Gökberk 2019).

Weight loss (%)

The weight loss percentage was calculated using the following formula:

$$Weight\ loss\ (\%) = (W_B - W_F/W_b) \times 100 \quad (7)$$

Where

W_b = Initial dry weight of the fabric sample (before burial)

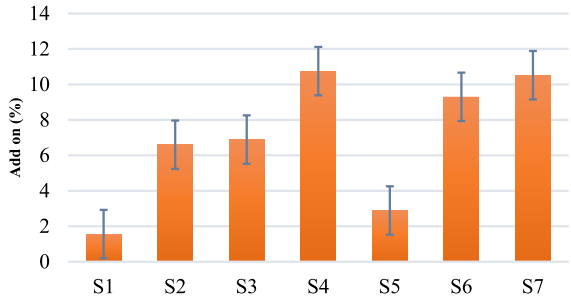

Fig. 3 Sericin add on percentage for nonwoven samples

W_f = Final dry weight of the fabric sample (after burial and drying)

Results and discussion

Sericin add-on (%)

The sericin add-on percentage presented in Fig. 3 shows varied significantly across the seven tested samples (S1–S7), reflecting the impact of different fiber composition on sericin deposition. S4 exhibited the highest add-on value (10.8%), followed closely by S7 (10.5%) and S6 (9.3%), indicating superior coating efficiency in these samples. Moderate values were observed in S2 (6.5%) and S3 (6.8%), while S1 (1.6%) and S5 (3.0%) showed the lowest sericin uptake. The error bars in the graph denote standard deviations, indicating the consistency of the results within each group. Statistical analysis using one-way ANOVA confirmed a significant difference among the groups ($p < 0.05$), and Tukey's post-hoc test revealed that S4 and S7 were statistically superior not only to S1 and S5 but also significantly different from S2 and S3. This clearly demonstrates that fiber composition led to more effective sericin adherence on nonwoven fabric surfaces.

Fourier transform infrared spectroscopy analysis

The FTIR spectra of raw fibers, identifying key functional groups within the 500 cm^{-1} to 4000 cm^{-1} range is illustrated Fig. 4 (a). A prominent absorption peak at 3313 cm^{-1} corresponds to O–H stretching vibrations, indicating the presence of hydroxy groups,

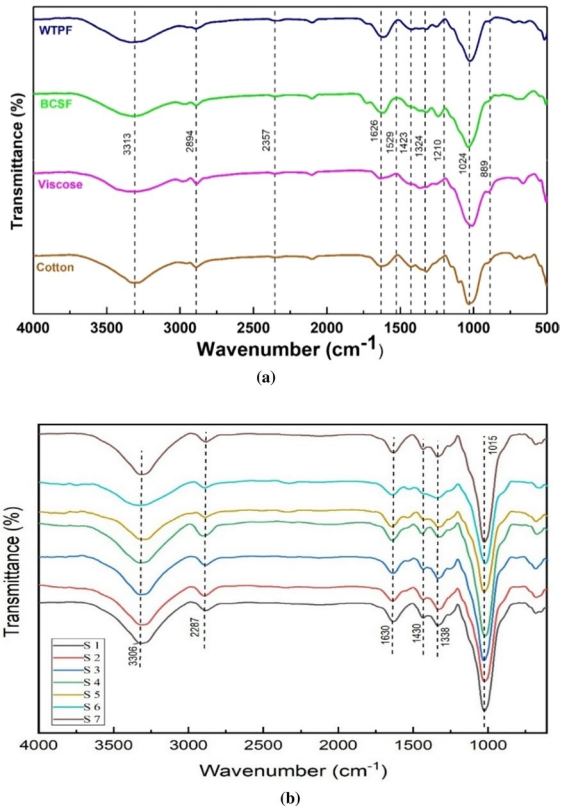

Fig. 4 (a): FTIR spectra of raw fibers (Cotton, viscose, banana core stem fiber, and wild turmeric petiole fiber. (b): Adhesive-bonded nonwoven fabrics

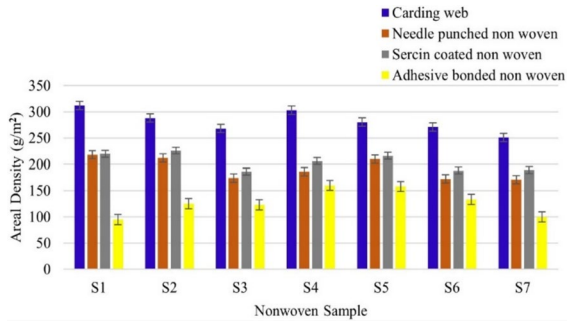

Fig. 5 Areal density of nonwoven fabrics

which are characteristic of cellulose-rich fibers (Kumar et al. 2022) (Ahmed et al. 2021). The peak at 2894 cm^{-1} is attributed to aliphatic C–H stretching vibrations from CH and CH_2 groups, confirming the presence of cellulose and hemicellulose components, particularly in viscose (Balasundar et al. 2018). Additionally, a peak at 2357 cm^{-1} suggests the presence of wax or wax-like substances (Maheshwaran et al. 2018).

The 1626 cm^{-1} peak corresponds to C=O stretching in hemicelluloses, which may also indicate lignin presence in plant-based fibers (Manimaran et al. 2020). The 1529 cm^{-1} peak is associated with aromatic C=C stretching in lignin (Joe et al. 2023). Cotton exhibits weaker absorbance, with a 1423 cm^{-1} peak linked to CH_2 stretching in cellulose (Senthamaraikannan and Kathiresan 2018). The 1324 cm^{-1} peak corresponds to C–H bending and C–O stretching in polysaccharides (Balasundar et al. 2018), while 1210 cm^{-1} represents C–O–C stretching in polysaccharides (Senthamaraikannan and Kathiresan 2018). The 1024 cm^{-1} peak is attributed to symmetric C–OH stretching in lignin (Senthamaraikannan et al. 2019), whereas the 889 cm^{-1} peak indicates C–OH stretching vibrations (Manimaran et al. 2018).

The FTIR spectra of adhesive-bonded nonwoven fabrics, highlighting the presence of sericin coating presents Fig. 4 (b). The peak at 3306 cm^{-1} corresponds to amide N–H stretching vibrations, confirming the presence of protein-linked N–H bonds. The 1630 cm^{-1} peak represents the amide I band, primarily associated with C=O stretching, while the 1530 cm^{-1} peak corresponds to the amide II band, reflecting N–H bending and C-N stretching vibrations.

The 1430 cm^{-1} peak is linked to C-H bending vibrations, typically associated with alkyl groups in the sericin structure. The 1338 cm^{-1} peak represents the amide III band, which corresponds to C-N stretching and N–H bending vibrations. These characteristic peaks confirm the successful incorporation of sericin into the nonwoven fabric structure, enhancing its protein content (Gün Gök et al. 2020).

Areal density

Areal density, a key parameter influencing the physical performance of nonwoven fabrics, was measured at different stages of nonwoven fabrication, as shows in Fig. 5.

The carded web exhibited the highest areal density, ranging from 251 to 312 g/m^2 ($F=338.211$; $p=0.000$), indicating significant variation between the samples. This higher areal density can be attributed to the uniform fiber arrangement and

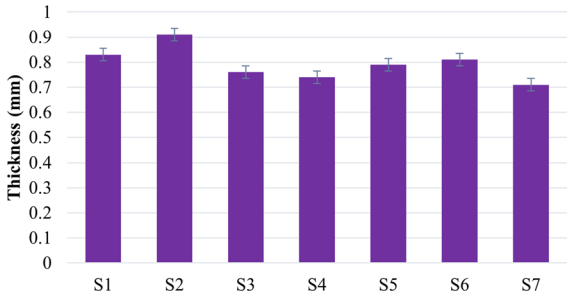

Fig. 6 Thickness of adhesive bonded nonwoven fabric

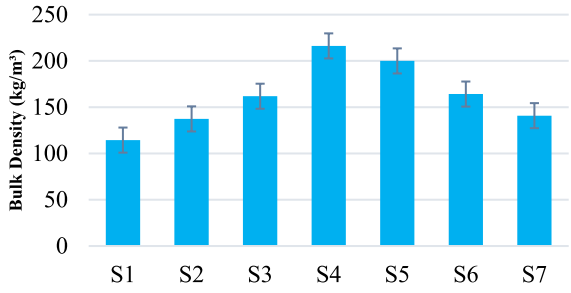

Fig. 7 Bulk density of adhesive-bonded nonwoven fabric samples

entanglement within the web formation process. The needle-punched nonwoven fabrics exhibited a lower areal density, ranging from 171 to 218 g/m^2, with statistically significant differences ($F=8.558$; $p=0.000$). The relatively lower values result from the mechanical fiber entanglement process, which increases porosity while maintaining fabric integrity.

The sericin-coated nonwoven fabrics exhibited slightly higher areal density values, ranging from 186 to 226 g/m^2, also showing statistical significance ($F=5.208$; $p=0.000$). The increase in density is likely due to the deposition of sericin on the fabric surface, which enhances fiber binding and reduced inter-fiber voids.

Among all samples, the adhesive-bonded nonwoven fabrics had the lowest areal density, ranging between 95 and 160 g/m^2, yet maintaining statistical significance ($F=12.462$; $p=0.000$). This lower areal density may be due to the adhesive bonding process, which relies on localized bonding points rather than a uniform fiber network, leading to a more open structure.

These results confirm that different treatments significantly influence the areal density. Higher areal density generally correlates with increased fabric strength and durability, making carded and sericin-coated fabrics more suitable for applications requiring enhanced mechanical properties. In contrast, adhesive-bonded nonwovens, with their lower areal density, may be more appropriate for applications requiring flexibility and breathability.

Thickness

The thickness characteristics of adhesive-bonded nonwoven fabrics are summarized in Fig. 6. The results indicate significant difference in thickness among the samples, except for S1, which did not show statistically significant variation ($F=2.403$; $p=0.084$). S2 exhibited the highest thickness (0.91 ± 0.06 mm) with statistically significant variation ($F=7.326$; $p=0.001$), followed by S3 (0.76 ± 0.12 mm, $F=6.762$; $p=0.001$). S4 showed a slightly lower thickness (0.74 ± 0.09 mm), yet displayed strong statistically significant ($F=10.318$; $p=0.000$). S5 had a moderate thickness value (0.79 ± 0.09 mm, $F=3.635$; $p=0.022$), while S6 exhibited a relatively high or thickness (0.81 ± 0.14 mm), showing the most pronounced statistical significance ($F=23.018$; $p=0.000$). S7 recorded the lowest thickness (0.71 ± 0.13 mm), with substantial variation ($F=10.811$; $p=0.000$). These findings highlight the significant influence of the adhesive bonding process on fabric thickness.

Bulk density

The bulk density of adhesive-bonded nonwoven fabrics, as shown in Fig. 7, varies significantly across samples, indicating the influence of different fiber ratios on material compactness. The bulk density of the adhesive-bonded nonwoven fabric samples (S1–S7) varied significantly, ranging from 114.46 kg/m^3 (S1) to 216.22 kg/m^3 (S4), with an overall mean of 162.06 kg/m^3 and a standard deviation of approximately 331.87 kg/m^3. These results reveal substantial

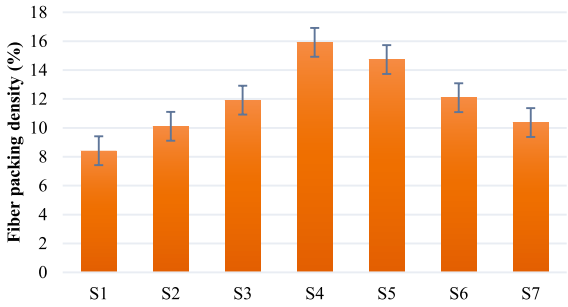

Fig. 8 Fiber packing density of adhesive bonded nonwoven samples

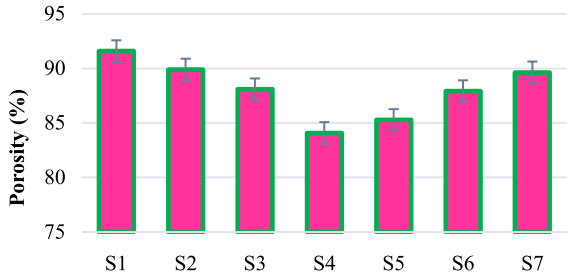

Fig. 9 Porosity of adhesive bonded nonwoven fabrics

variation in the compactness and porosity of the nonwoven structures, largely by adhesive application, bonding pressure, and fiber distribution. Among all samples, S4 demonstrated the highest bulk density (216.22 kg/m^3), indicating the most compact and least porous structure, possibly due to higher adhesive penetration and stronger bonding force during the manufacturing process. S5 followed S4 closely with a bulk density of 200.00 kg/m^3, reinforcing its status as a dense and robust fabric, likely suitable for applications requiring durability and strength.

Sample S6 also exhibited a relatively high bulk density (164.53 kg/m^3), suggesting better fiber consolidation than S1, S2, or S7, though less than S4 and S5. S3, with a density of 161.11 kg/m^3, ranked in the upper mid-range and could be considered moderately compact with balanced strength and flexibility. In the mid-to-lower density range, S2 and S7 recorded values of 137.64 kg/m^3 and 140.07 kg/m^3 respectively. These results suggest a more open fiber structure, potentially improving softness, air permeability, or moisture absorption. However, their reduced density may limit mechanical strength in high-stress applications.

S1, with the lowest bulk density (114.83 kg/m^3), stands out as the most porous and loosely bonded sample. This likely results from minimal adhesive application or lower compression force, making it potentially suitable for uses where breathability or softness is prioritized over structural strength. A one-way ANOVA analysis confirmed that these differences in bulk density across samples were statistically significant ($F = 5.432$; $p < 0.01$), reinforcing the impact of processing conditions on the fabric. Higher bulk density correlates with greater strength, stiffness, and reduced porosity. Lower-density fabrics may be preferred in products requiring comfort, breathability, or absorbency, such as hygiene or medical textiles.

Fiber packing density

The fiber packing density (%) of adhesive-bonded nonwoven samples (S1–S7), as presented in Fig. 8. An increasing pattern is observed from S1 (8.42%) to S4 (15.92%), indicating enhanced fiber consolidation and effective adhesive bonding up to this point. S4 records the highest packing density, suggesting optimal bonding conditions. Beyond this, a gradual decline is seen in S5 (14.73%), S6 (12.09%), and S7 (10.37%), possibly due to reduced bonding efficiency or changes in fabric structure. The minimal and consistent error bars across all samples reflect high measurement precision. One-way ANOVA results confirm that the differences in fiber packing density among the samples are statistically significant ($p < 0.05$). Further analysis using Tukey's post hoc test revealed that S4 had significantly higher packing density than S1, S2, and S7 ($p < 0.05$), highlighting its superior structural integrity. Overall, these findings suggest that sample S4 provides the most effective combination of fiber orientation and adhesive application.

Porosity

The porosity of adhesive-bonded nonwoven fabric samples (S1–S7), shown in Fig. 9, illustrates the percentage of void space within each material. The porosity values range from a maximum of 91.58% in S1 to a minimum of 84.08% in S4. A gradual decrease is observed from S1 through S4, followed by a slight increase from S5 (85.27%) to S7 (89.63%).

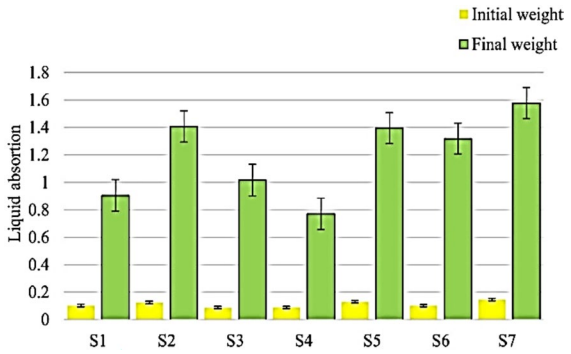

Fig. 10 Liquid absorption of adhesive-bonded nonwoven fabrics

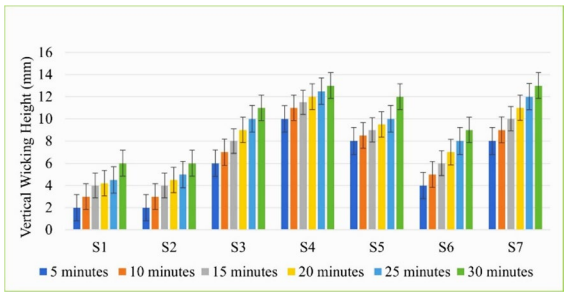

Fig. 11 Vertical wicking performance of adhesive-bonded nonwoven fabrics

This pattern reflects changes in fiber arrangement and compaction across the samples. High porosity is generally associated with enhanced air and fluid permeability, which is desirable for applications like filtration, insulation, and hygiene products.

The relatively small error bars across all samples indicate consistent measurements. Statistical analysis using one-way ANOVA revealed no significant differences in porosity among the samples ($p > 0.05$), confirming the uniformity in void distribution despite differences in fiber bonding.

From an application perspective, samples like S1 and S7, with higher porosity, are better suited for breathable fabrics such as face masks and absorbent materials. Samples with moderate porosity (S2, S3, S6) offer a balance between permeability and structural integrity, making them ideal for protective textiles and geotextiles. Meanwhile, samples like S4 and S5, with relatively lower porosity, provide greater fiber compactness and durability, suitable for industrial or load-bearing applications. Overall, the consistent porosity across samples highlights their suitability for targeted functional uses in filtration, medical, and technical textiles.

Liquid absorption

The liquid absorption results for nonwoven fabric samples S1 through S7, highlighting significant differences in their water retention capacities illustrated Fig. 10. Sample S7 exhibited the highest absorption, increasing from an initial weight of 0.1456 g to a final weight of 1.5764 g, indicating superior absorbency. Similarly, Sample S2 showed a substantial increase from 0.1238 g to 1.4068 g, followed by Sample S5 (0.1296 g to 1.3944 g) and Sample S6 (0.1016 g to 1.3180 g). Sample S3 demonstrated moderate absorption, rising from 0.0872 g to 1.0154 g. In contrast, Sample S4 recorded the lowest absorption, increasing from 0.0874 g to 0.7710 g, indicating relatively low absorbency.

A paired t-test for Sample S1 revealed a highly significant difference ($t = -10.224$; $p < 0.001$), confirming notable water absorption changes. These results emphasize the varying absorption capacities of the materials, reflecting differences in their structural or compositional properties. These absorption characteristics is crucial for applications where liquid management is essential, such as in medical textiles, hygiene products, and absorbent materials.

Vertical wicking

The vertical wicking behaviour of adhesive bonded nonwoven fabric samples (S1–S7) over different time intervals (5, 10, 15, 20, 25, and 30 min) shows Fig. 11. Vertical wicking, which refers to the upward movement of liquid through a material due to capillary action, is a crucial property for applications such as wipes, diapers, and medical textiles.

The results indicate significant differences in vertical wicking performance among the samples. Sample S4 exhibited the highest wicking ability across all time points, with the liquid reaching the greatest height at each interval. Samples S5 and S7 also demonstrated strong wicking performance, with steady liquid movement over time. In contrast, Sample S1 exhibited the lowest wicking height, indicating limited capillary action and slower liquid transport.

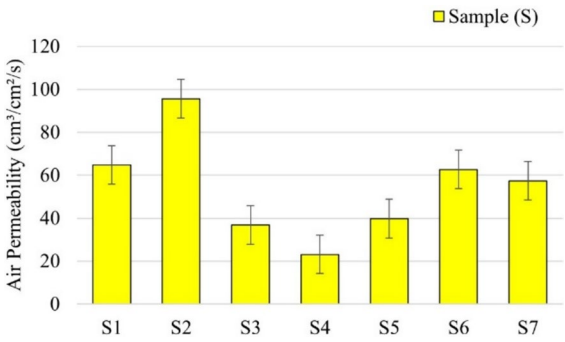

Fig. 12 Air permeability of adhesive bonded nonwoven fabrics

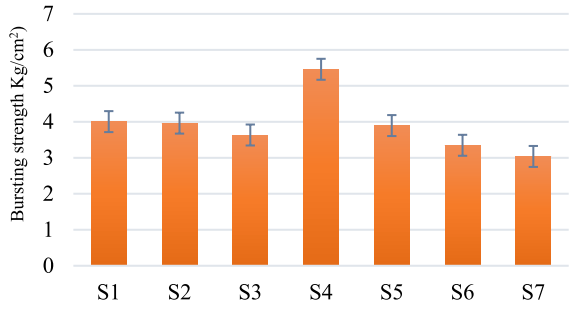

Fig. 13 Bursting strength of adhesive bonded nonwoven fabric

Statistical analysis revealed a significant variation in wicking performance among the samples. The mean wicking height at 30 min ranged from 5.8 mm (S1) to 13.4 mm (S4), with a standard deviation of ± 0.72 mm. A one-way ANOVA test showed a statistically significant difference between the samples ($p < 0.05$), confirming that fiber composition and structural properties influence the wicking behaviour.

Air permeability

Air permeability results across the study samples showed considerable variation (Fig. 12). S2 exhibited the highest air permeability value of 95.62 $cm^3/cm^2/s$, indicating a significantly more porous structure compared to the others. In contrast, S4 recorded the lowest air permeability of 23.12 $cm^3/cm^2/s$, suggesting a denser or less porous material, which may result from tighter fiber bonding or reduced pore size. Samples S1 (64.79 $cm^3/cm^2/s$), S6 (62.7 $cm^3/cm^2/s$), and S7 (57.43 $cm^3/cm^2/s$) exhibited relatively high air permeability, whereas S3 (36.8 $cm^3/cm^2/s$) and S5 (39.79 $cm^3/cm^2/s$) demonstrated moderate values.

Statistical analysis revealed a significant difference in air permeability across the samples ($F = 18.54$, $p < 0.001$), confirming that variations in material structure play a crucial role in airflow regulation. The standard deviations across the samples further highlight the variability in permeability, with S7 showing the highest variation, indicating potential inconsistencies in material formation.

These findings emphasize the impact of fiber composition, processing methods, and structural bonding on air permeability. The higher permeability observed in S2 suggests it could be suitable for applications requiring enhanced breathability, such as medical or filtration textiles. Conversely, the lower permeability of S4 might be beneficial in barrier applications where restricted airflow is desired.

Bursting strength

The bursting strength of the nonwoven fabric samples (S1–S7) was evaluated and is presented in Fig. 13. Among all samples, S4 exhibited the highest bursting strength, indicating superior resistance to rupture under multi-directional stress. Samples S1, S2, and S5 showed moderate values, while S3, S6, and S7 displayed comparatively lower bursting strength. This variation can be attributed to differences in fiber blend composition and presence of sericin coating bonding mechanism.

To determine the statistical significance of these differences, a one-way analysis of variance (ANOVA) was conducted. The ANOVA results revealed a statistically significant difference in bursting strength values among the samples ($p < 0.05$), indicating that the type of fiber blend and finishing treatments significantly influence the mechanical performance of the nonwovens. Further pairwise comparisons using tukey's HSD post-hoc test identified S4 as significantly different ($p < 0.05$) from the other groups, reinforcing its superior mechanical integrity.

Additionally, independent sample t-tests were applied to selected pairs (e.g., S4 vs. S3 and S4 vs. S7), confirming that the improvements in S4 were statistically significant. The findings highlight the potential of the specific fiber composition and bonding technique used in S4 for enhancing the strength of

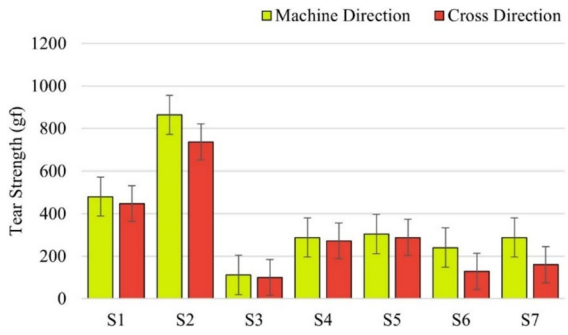

Fig. 14 Tear strength of adhesive bonded nonwoven fabric

nonwoven fabric, making it suitable for applications requiring high mechanical durability.

Tear strength

The tear strength results across the samples, measured in both the machine direction (MD) and cross direction (CD), highlighting significant variations summarized Fig. 14. S2 exhibited the highest tear strength in both directions, with 864 gf in MD and 736 gf in CD, indicating superior durability and resistance. S1 followed with relatively high values (480 gf in MD and 448 gf in CD), and statistical analysis showed a significant difference ($t = 3.284$, $p = 0.017$).

Samples S4 and S5 demonstrated moderate tear strength values in both directions, suggesting a balanced structural performance. In contrast, S3 (112 gf in MD, 80 gf in CD) and S7 (288 gf in MD, 160 gf in CD) recorded the lowest values, while S6 exhibited the weakest tear strength in the cross direction (128 gf), indicating lower resistance in that orientation.

The statistical analysis confirmed significant differences in tear strength across the samples, $p < 0.05$, if available), emphasizing the influence of structural orientation, fiber bonding, and material composition on mechanical performance. These findings suggest that materials with higher tear strength, such as S2 and S1, may be more suitable for applications requiring enhanced durability, while lower-performing samples may require structural reinforcement for improved performance.

Surface morphology

Field Emission Scanning Electron Microscope (FESEM) images of adhesive-bonded nonwoven fabrics (S1–S7) at magnifications ranging from 100 µm to 10 µm, highlighting the fiber morphology and surface textures of the composite structures shows Fig. 15. Cotton fibers display a characteristic ribbon-like, twisted morphology with relatively smooth surfaces, while viscose fibers appear uniform and cylindrical, reflecting their regenerated cellulose origin. Banana core stem fibers exhibit a stratified structure with prominent surface striations, indicative of their lignocellulosic nature. Wild turmeric petiole fibers are densely packed, irregular, and coarse, with a complex texture. In S1, fibers are randomly oriented, intertwined, and occasionally frayed, with diameters ranging from approximately 10 to 25 µm. S2 features flattened, ribbon-like fibers with evident surface roughness and microfractures, measuring between 8 and 20 µm. Sample S3 contains loosely arranged and frayed fibers with thickness variations (12–22 µm), while S4 shows knotted or coiled fibers with smooth, cylindrical surfaces measuring 10–15 µm. The fibers in S5 are twisted, interwoven, and irregular in appearance, with widths ranging from 15 to 30 µm. S6 reveals a densely layered and compact structure, with fiber widths between 18 and 28 µm, marked by surface roughness and micro-cracking. S7 displays thin, elongated fibers with fine striations and random orientations, measuring 8–14 µm in diameter. These morphological features directly influence the mechanical interlocking and adhesion characteristics of the composites, potentially impacting their performance in sustainable material applications.

pH analysis of adhesive bonded nonwoven fabric

The developed adhesive bonded nonwoven fabric samples exhibit pH values in the range of 6.63 to 6.96 (Table 2), indicating a near-neutral to mildly acidic surface environment. This pH range is generally regarded as safe and compatible with human skin, making the nonwoven fabrics particularly suitable for personal care applications such as cosmetic wipes, face wipes, baby wipes, and kitchen wipes where skin contact is frequent.

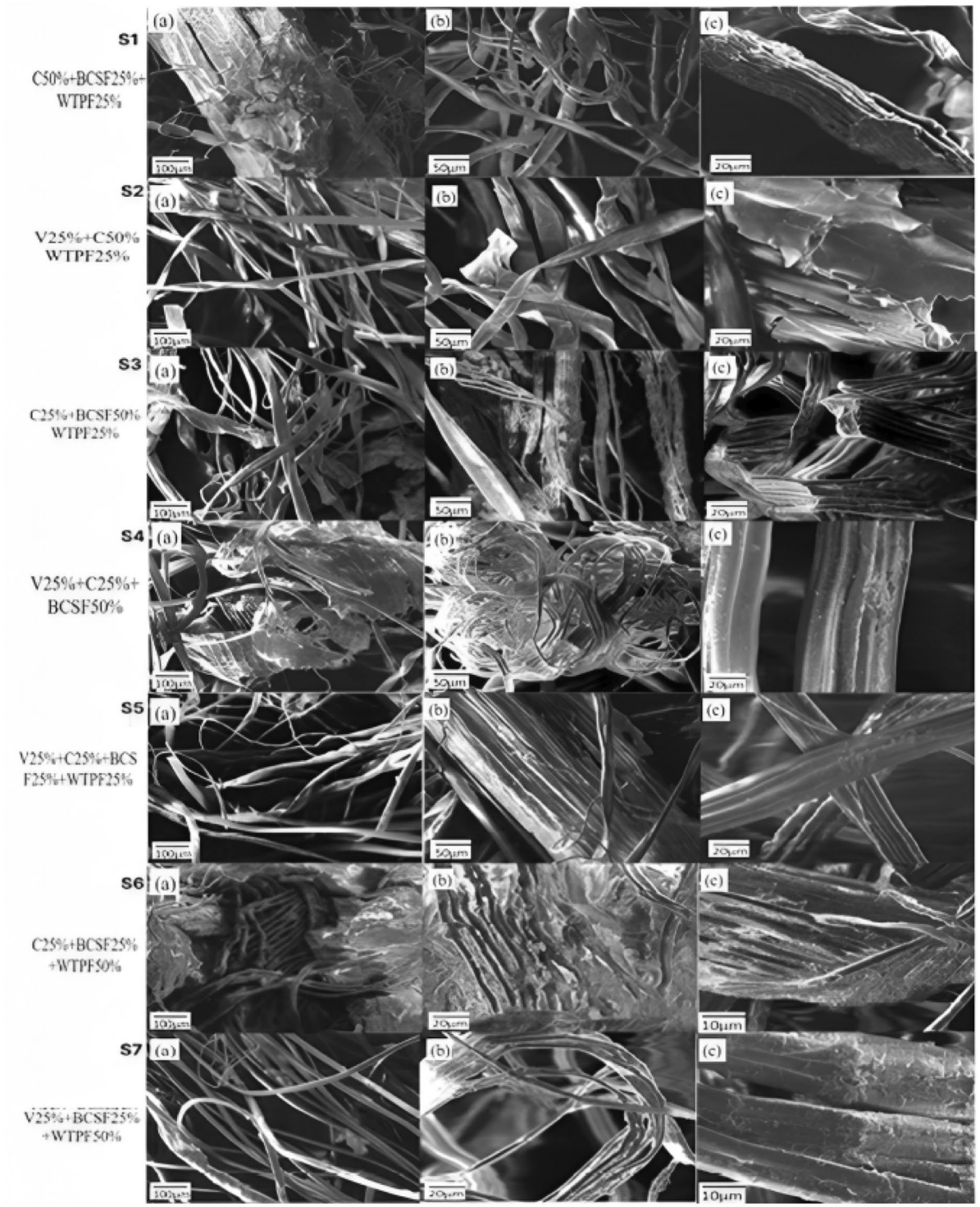

Fig. 15 Morphological analysis of adhesive bonded nonwoven fabrics a)100 µm b) 50 µm c) 20–10 µm. V-viscose C- cotton, BCSF- banana core stem fiber WTPF- wild turmeric petiole fiber

Table 2 pH values for adhesive bonded nonwoven fabrics

Sample	pH
S1	6.96
S2	6.58
S3	6.96
S4	6.63
S5	6.58
S6	6.60
S7	6.69

Soil burial analysis

The soil burial test results revealed a gradual and significant degradation of the adhesive bonded nonwoven fabrics over time. As shown in Fig. 16, all fabric samples (S1–S7) exhibited progressive decomposition across the burial periods of 30, 90, and 120 days.

0 Day (Control): All samples retained their original structure, shape, and texture, with no visible signs of degradation. 30 Days: Initial signs of microbial degradation were observed. Structural weakening, fraying, and edge breakdown were evident, particularly in samples S2, S3, and S6. Minor color fading and surface deterioration were also noticeable.

90 Days: The fabrics showed severe structural disintegration and fragmentation. Samples such as S3, S4 and S5 lost most of their integrity, while others exhibited advanced breakdown with loose fibrous residues. 120 Days: All samples were completely decomposed, confirming full biodegradation under natural soil conditions.

Weight loss (%)

The biodegradation of the adhesive bonded nonwoven fabric samples was quantitatively assessed based on weight loss (%) after 30 and 90 days of soil burial. As shown in Fig. 17 all samples (S1–S7) exhibited substantial weight loss, confirming ongoing microbial degradation under natural soil conditions.

After 30 days, the weight loss ranged from 15% to 66%, with S5 showing the highest degradation (66%) followedby S3 and S1 (55% and 52%, respectively). Samples S6 and S7 exhibited the lowest degradation at this stage, with weight loss below 25%, suggesting slower degradation possibly due to their composition or structural density. After 90 days of soil burial, a significant increase in biodegradation was observed across all samples. The weight loss ranged from 63% to 90%, with S5 and S7 achieving the highest degradation (90%), indicating excellent biodegradability. Samples S2, S4, and S1 also demonstrated high weight loss (85–88%), while S6 remained the least degraded (63%), though it still showed substantial improvement compared to the 30-day value. Statistical analysis using one-way ANOVA confirmed that the differences in mean weight loss among the samples were significant ($p < 0.05$). The overall results confirm the biodegradability of the nonwoven fabrics, with variations attributed to differences in fiber composition such as cotton, viscose, banana core stem fiber (BCSF), and wild turmeric petiole fiber (WTPF), bonding method, and structural characteristics. By 120 days, all samples were completely decomposed, leaving no visible residue in the soil. This confirms that the developed nonwoven fabrics are fully biodegradable under natural conditions and hold strong potential for sustainable applications, including wet wipes, eco-friendly packaging, and disposable textiles.

Conclusion

In this study explores the feasibility of utilizing agro-waste fibers, specifically banana core stem fiber (BCSF) and wild turmeric petiole fiber (WTPF), in developing nonwoven fabrics for technical textile applications including hygiene, agricultural, geotextile, and industrial use. The characterization results revealed distinct differences in fabric properties, which are attributed to the inherent structural and physical variations in the blended fibers. For instance, S1 (Cotton 50%, BCSF 25%, WTPF 25%) exhibited light weight and high air permeability, making it suitable for hygiene disposables such as wipes and liners—properties likely due to the presence of finer cotton fibers and lower bulk density. S2 (Cotton 50%, Viscose 25%, WTPF 25%) showed the highest tensile and tear strength, attributed to viscose's uniformity and WTPF's supportive structure, making it ideal for agro-textiles and geotextiles requiring mechanical durability. S3 (Cotton 25%, BCSF 50%, WTPF 25%) had a more open structure with moderate absorbency, influenced by the coarser BCSF content, suggesting suitability for biodegradable packaging. S4 (Viscose

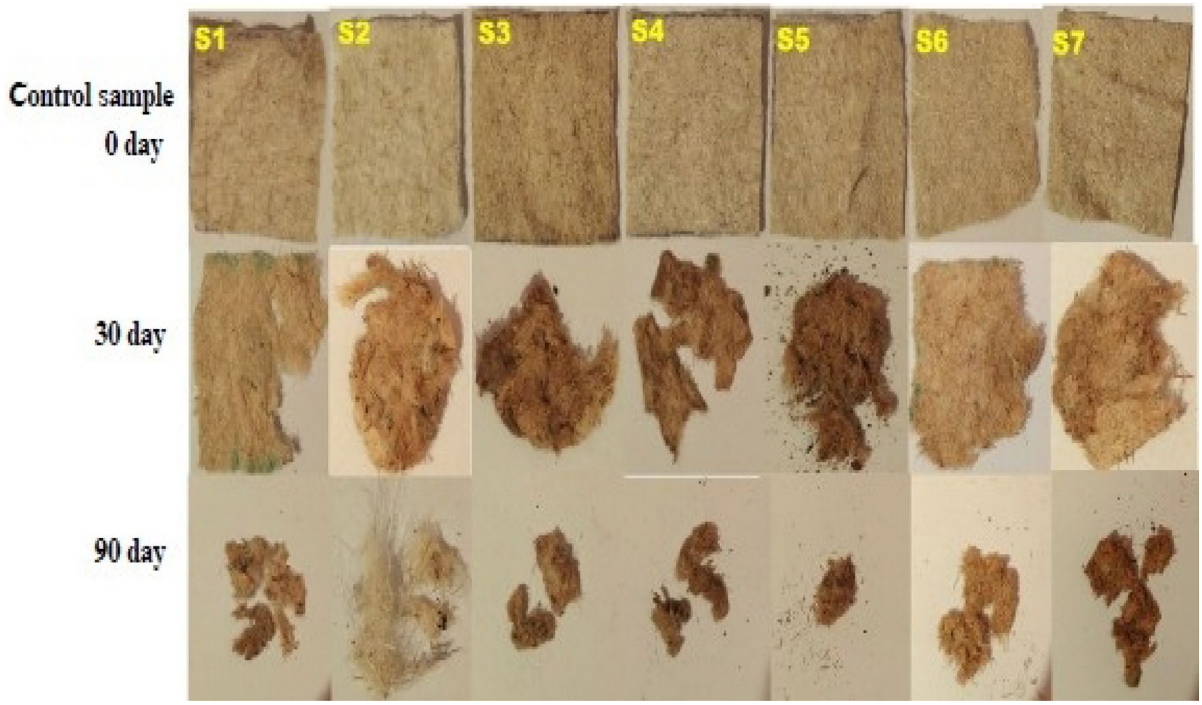

Fig. 16 Visual representation of degradation in adhesive bonded nonwoven fabric samples (S1–S7) after 0, 30, and 90 days of soil burial

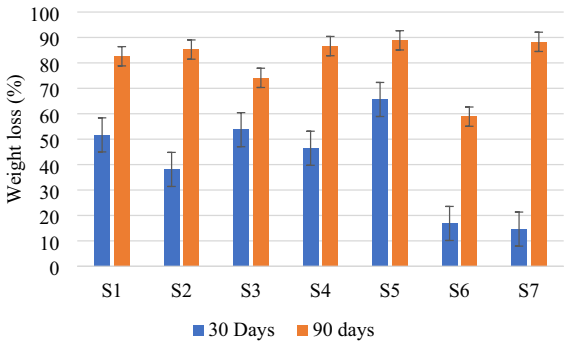

Fig. 17 Weight loss (%) of adhesive bonded nonwoven fabrics after soil burial at 30 and 90 days

25%, Cotton 25%, BCSF 50%) displayed the highest bursting strength and packing density, likely due to BCSF's higher fiber stiffness and increased fabric compactness—indicating potential for barrier textiles and protective materials. S5 (Viscose 25%, Cotton 25%, BCSF 25%, WTPF 25%) exhibited balanced properties suitable for medical textiles and insulation. S6 and S7, which had a 50% WTPF blend, showed the highest porosity and capillarity due to WTPF's hollow structure and wicking ability—S6 (Cotton-based) suited for filtration, and S7 (Viscose-based) ideal for absorbent hygiene products and horticultural mats. These results confirm that fiber type and blend ratio significantly influence fabric performance. By correlating fiber morphology with functional outcomes, the study supports targeted end-use recommendations. Utilizing agro-waste fibers not only substitutes synthetic materials but also advances circular economy goals through valorization of biodegradable, renewable resources. Future work will focus on manufacturing, scalability, long-term durability, biodegradability under real-use conditions, and industrial adoption.

Author contribution Author contribution Ramya Kanagaraj > > Experiment, Analysis, Original draft writing Amutha Karuppuchamy > > Conceptualization, Supervision, Editing Sukanya Devi Ramachandran > > Methodology.

Funding The work is not supported by any external funding agency.

Data availability No datasets were generated or analysed during the current study.

Declarations

Conflict of interest The authors declare no competing interests.

Ethical approval This article does not involve any human subjects.

References

Ahmed J, Balaji MA, Saravanakumar SS, Senthamaraikannan P (2021) A comprehensive physical, chemical and morphological characterization of novel cellulosic fiber extracted from the stem of *Elettaria cardamomum* plant. J Nat Fibers 18:1460–1471. https://doi.org/10.1080/15440478.2019.1691121

Amutha K, Sudha A, Saravanan D (2020) Characterization of Natural Fibers Extracted from Banana Inflorescence Bracts Characterization of Natural Fibers Extracted from Banana Inflorescence Bracts. J Nat Fibers 00:1–10. https://doi.org/10.1080/15440478.2020.1764437

Balasundar P, Narayanasamy P, Senthamaraikannan P et al (2018) Extraction and Characterization of New Natural Cellulosic Chloris barbata Fiber. J Nat Fibers 15:436–444. https://doi.org/10.1080/15440478.2017.1349015

Bhat G, Parikh D V. (2010) Biodegradable materials for nonwovens. Appl Nonwovens Tech Text 46–62. https://doi.org/10.1016/B978-1-84569-437-1.50003-3

Elnashar EA (2005) Volume porosity and permeability in double-layer woven fabrics. AUTEX Res J 5:207–218. https://doi.org/10.1515/aut-2005-050404

Fatahian R, Khajavi R, Branch ST (2018) Exrtaction of sericin from degumming process of silk fibres and its application on nonwoven fabrics. https://doi.org/10.14419/ijac.v5i1.7416

Gaminian H, Ahvazi B, Vidmar JJ et al (2024) Revolutionizing Sustainable Nonwoven Fabrics: The Potential Use of Agricultural Waste and Natural Fibres for Nonwoven Fabric. Biomass (Switzerland) 4:363–401. https://doi.org/10.3390/biomass4020018

Govindaraju R, Jagannathan S (2018) Certain Properties of Needle Punched Nonwoven Fabrics Made from Silk and Wool Fibers. 1:28–31. https://doi.org/10.31031/TTEFT.2018.01.000507

Gün Gök Z, Günay K, Arslan M et al (2020) Coating of modified poly(ethylene terephthalate) fibers with sericin-capped silver nanoparticles for antimicrobial application. Polym Bull 77:1649–1665. https://doi.org/10.1007/s00289-019-02820-0

Jhanji Y, Gupta D, Kothari VK (2015) Thermo - physiological properties of polyester – cotton plated fabrics in relation to fibre linear density and yarn type. Fash Text. https://doi.org/10.1186/s40691-015-0041-x

Joe MS, Sahaya DP, Indran S, Suchart S (2023) Extraction and characterization of novel biomass – based cellulosic plant fiber from Ficus benjamina L . stem for a potential polymeric composite reinforcement. Biomass Convers Biorefinery. https://doi.org/10.1007/s13399-023-03759-z

Karuppuchamy A, K. R, R. S (2024) Novel banana core stem fiber from agricultural biomass for lightweight textile applications. Ind Crops Prod 209:117985. https://doi.org/10.1016/j.indcrop.2023.117985

Kim YE, Bae YJ, Jang MJ (2023) Effect of Sericin Content on the Structural Characteristics and Properties of New Silk Nonwoven Fabrics

Kumar R, Sivaganesan S, Senthamaraikannan P et al (2022) Characterization of New Cellulosic Fiber from the Bark of Acacia nilotica L. Plant J Nat Fibers 19:199–208. https://doi.org/10.1080/15440478.2020.1738305

Maheshwaran MV, Hyness NRJ, Senthamaraikannan P et al (2018) Characterization of natural cellulosic fiber from Epipremnum aureum stem. J Nat Fibers 15:789–798. https://doi.org/10.1080/15440478.2017.1364205

Manimaran P, Sanjay MR, Senthamaraikannan P et al (2020) A new study on characterization of Pithecellobium dulce fiber as composite reinforcement for light-weight applications. J Nat Fibers 17:359–370. https://doi.org/10.1080/15440478.2018.1492491

Manimaran P, Senthamaraikannan P, Murugananthan K, Sanjay MR (2018) Physicochemical Properties of New Cellulosic Fibers from Azadirachta indica Plant. J Nat Fibers 15:29–38. https://doi.org/10.1080/15440478.2017.1302388

Mao N, Russell SJ (2015) Fibre to Fabric: Nonwoven Fabrics. Elsevier Ltd

Mitchell R-L (2019) Causes, effects and solutions of operational problems in wastewater systems due to nonwoven wet wipes

Nivedita and Mishra (2016) Novel Applications of Silk Nonwovens in Living Enclosures. 1–4

Ramya Kanagaraj & Amutha Karuppuchamy (2024) Characterization of Ligno-cellulosic fibers from Wild turmeric (Curcuma aromatica) petiole for potential textile applications. Cellulose. https://doi.org/10.1007/s10570-024-06211-1

Santos AS, Maloney PJTFT, Jose R (2021) Bio-based materials for nonwovens. Springer, Netherlands

Senthamaraikannan P, Kathiresan M (2018) Characterization of raw and alkali treated new natural cellulosic fiber from *Coccinia grandis*.L. Carbohydr Polym 186:332–343. https://doi.org/10.1016/j.carbpol.2018.01.072

Senthamaraikannan P, Saravanakumar SS, Sanjay MR et al (2019) Physico-chemical and thermal properties of untreated and treated Acacia planifrons bark fibers for composite reinforcement. Mater Lett 240:221–224. https://doi.org/10.1016/j.matlet.2019.01.024

Shaikh TN, Chaudhari SB, Panchal R, Patel BH (2023) Hygiene characterization of polypropylene nonwoven composites produced on loading bio synthesized silver nanoparticles using Aloe Barbadensis Miller plant extract.

Hybrid Adv 2:100032. https://doi.org/10.1016/j.hybadv.2023.100032

Sülar V, Devrim G (2019) Biodegradation Behaviour of Different Textile Fibres: Visual , Morphological, Structural Properties and Soil Analyses 1:100–111. https://doi.org/10.5604/01.3001.0012.7751

Temesgen AG (2018) Process Ability Enhancement of False Banana Fibre for Rural Development. https://doi.org/10.13140/RG.2.2.36612.01926

Thilagavathi G, Muthukumar N, Neela Krishnanan S, Senthilram T (2020) Development and characterization of pineapple fibre nonwovens for thermal and sound insulation applications. J Nat Fibers 17:1391–1400. https://doi.org/10.1080/15440478.2019.1569575